A novel approach for simulating multi-component and multi-phase flow using free energy and multiple distribution functions in lattice Boltzmann method

Zhonghua Qiao[a,*], Xuguang Yang[b,*], Yuze Zhang[c]

[a] *Department of Applied Mathematics, The Hong Kong Polytechnic University, Hung Hom, Hong Kong*
[b] *School of Mathematics and Statistics, Hunan First Normal University, Changsha, P. R. China*
[c] *School of Mathematical Sciences, Nanjing Normal University, Nanjing, China*

Abstract

This study presents the development of a multiple-distribution-function lattice Boltzmann model (MDF-LBM) for the accurate simulation of multi-component and multi-phase flow. The model is based on the diffuse interface theory and free energy model, which enable the derivation of hydrodynamic equations for the system. These equations comprise a Cahn-Hilliard (CH) type mass balance equation, which accounts for cross diffusion terms for each species, and a momentum balance equation. By establishing a relationship between the total chemical potential and the general pressure, the momentum balance equation is reformulated in a potential form. This potential form, together with the CH type mass balance equation, is then utilized to construct the MDF-LBM as a coupled convection-diffusion system. Numerical simulations demonstrate that the proposed MDF-LBM accurately captures phase behavior and ensures mass conservation. Additionally, the calculated interface tension exhibits good agreement with experimental data obtained from laboratory studies.

Keywords: multi-component and multi-phase flow, free energy model, lattice Boltzmann method

1. Introduction

Multi-component multi-phase flows are of great importance in natural phenomena and a variety of engineering applications, including reservoir engineering [1], environmental protection [2], and microfluidic chip design [3]. Accurate modeling and prediction of phase behavior are crucial for the success of these applications [4]. Over the years, various methods have been developed to describe the interface between different phases, such as the level set approach [5], front tracking method [6], volume of fluid method [7], diffuse interface method [8, 9, 10, 11], and so on. Among these methods, the diffuse interface method stands out for its ability to accurately capture interface curvature by considering the interface as thin but with non-zero thickness transitional regions. This method, along with others mentioned, has demonstrated success in numerically simulating multi-phase and multi-component fluid flow.

*Corresponding author
Email addresses: zhonghua.qiao@polyu.edu.hk (Zhonghua Qiao), xuguang1988@163.com (Xuguang Yang), 05439@njnu.edu.cn (Yuze Zhang)

The lattice Boltzmann method (LBM), rooted in kinetic theory, has demonstrated remarkable capabilities in simulating complex fluid flows [12, 13, 14, 15]. By incorporating the strengths of the diffuse interface model, various types of multi-phase and multi-component LBMs have been formulated [16, 17, 18, 19, 20, 21, 22]. These models can be broadly categorized into three groups: the pseudopotential model [23, 24], the free energy model [25, 26], and the phase field based model [27, 28]. Within the framework of the multi-component pseudopotential model, Deng et al. [29] presented an enhanced multi-component two-phase LBM by introducing a realistic equation of state (EOS) and scaling the original pressure with a defined scalar. This LBM has been shown to accurately simulate high density and viscosity ratios in multi-component two-phase systems. Additionally, Peng et al. [30] introduced a thermodynamically consistent multi-component, multiphase pseudo-potential LBM capable of predicting the phase behavior of partially miscible hydrocarbon mixtures. The free energy model, derived from the principles of thermodynamics, encompasses the non-ideal EOS within the pressure tensor of the Navier-Stokes (N-S) equations. Several enhancements have been made to refine the free energy model. One notable advancement is the development of a thermodynamically consistent free energy model for ternary multi-phase multi-component flows by W$\ddot{o}$hrwag et al. [9], which is based on the entropic LBM. In a similar vein, Ridl et al. [32] established an LBM framework specifically designed for simulating mixtures with a multi-component van der Waals EOS. Soomro [33] contributed to the field by introducing a free-energy LBM tailored for multi-component and multi-phase fluids with partial miscibility, where the forcing term is determined by the species' fugacity. Their work successfully simulated the vapor-liquid equilibrium of two- and three-component mixtures across various temperature and pressure conditions. Another commonly employed model for simulating multiphase flows is the phase field model, which uses an order parameter to track the distinct phases. This model is typically used for simulating multiphase flows involving N ($N \geq 2$) immiscible incompressible fluids [34, 35]. However, the thermodynamic properties of the phase field model are expressed using a double-well or multi-well free energy functional, limiting its ability to accurately mimic multi-component and multi-phase flows with realistic EOS.

In this study, we introduce a generalized multi-phase and multi-component free energy model to accurately capture the behavior of immiscible and partially miscible fluid systems with different EOS. The hydrodynamic equations used in this model, including the CH type mass conservation equation for each component and the potential form momentum balance equation, pose significant challenges for numerical methods. Building upon previous work [36], we have developed a coupled multiple-distribution-function lattice Boltzmann method (MDF-LBM) to effectively tackle these hydrodynamic equations, treating them as coupled convection-diffusion systems. The structure of this paper is as follows: In Section 2, we present the mathematical model and the hydrodynamic equations governing the behavior of multi-component and multi-phase system. In Section 3, we propose the MDF-LBM approach to solve the CH type mass conservation equation for each component and the potential form momentum balance equation. Section 4 demonstrates the validity and effectiveness of our numerical simulations. Finally, in Section 5, we make conclusions and engage in discussions pertaining to our findings.

2. Mathematical model of multi-component and multi-phase flow

In this section, we present a comprehensive mathematical model for multi-component two-phase fluids, which is based on the principles of multi-component free energy modeling and diffuse interface theory.

2.1. Helmholtz free energy

Consider the motion of a mixture fluid composed of M chemical components under a constant temperature (T). The molar density or volume fraction vector is denoted by $\mathbf{n} = [n_1, n_2, ..., n_M]^T$, where n_i is the molar density or volume fraction of component i. In the case of realistic fluids, the presence of diffuse interfaces between two phases requires an appropriate representation. To address this characteristic, the Helmholtz free energy of inhomogeneous fluids is supplemented with a term that incorporates local density gradients. The total Helmholtz free energy $F(\mathbf{n}; T, \Omega)$, consisting of two components: the Helmholtz free energy of the bulk homogeneous fluid $F_0(\mathbf{n}; T, \Omega)$ and a local density gradient term $F_\nabla(\mathbf{n}; T, \Omega)$, is given as follows.

$$F(\mathbf{n}; T, \Omega) = F_0(\mathbf{n}; T, \Omega) + F_\nabla(\mathbf{n}; T, \Omega) = \int_\Omega f_0(\mathbf{n}; T) d\mathbf{x} + \int_\Omega f_\nabla(\mathbf{n}; T) d\mathbf{x}. \tag{1}$$

Here, $f_0(\mathbf{n})$ is the Helmholtz free density of bulk homogeneous fluid, $f_\nabla(\mathbf{n})$ is the contribution of Helmholtz free energy density from the concentration gradient, which can be expressed as

$$f_\nabla(\mathbf{n}) = \frac{1}{2} \sum_{i,j=1}^{M} c_{ij} \nabla n_i \cdot \nabla n_j, \tag{2}$$

where c_{ij} represents the cross-influence parameter, which is associated with the thickness of the interface.

The chemical potential of component i is calculated as

$$\mu_i = (\frac{\delta f(\mathbf{n}, T)}{\delta n_i})_T = \mu_i^0 - \sum_{j=1}^{M} \nabla \cdot (c_{ij} \nabla n_j), \tag{3}$$

where $\delta / \delta n_i$ is the variational derivative and

$$\mu_i^0 = \frac{\partial f_0(\mathbf{n}, T)}{\partial n_i}. \tag{4}$$

Based on the fundamental principles of thermodynamics, the pressure of a homogeneous fluids, denoted as p_0, is related to $f_0(\mathbf{n})$ in the following way:

$$p_0 = p_0(\mathbf{n}, T) = \sum_{i=1}^{M} n_i (\frac{\partial f_0}{\partial n_i}) - f_0 = \sum_{i=1}^{M} n_i \mu_{0,i} - f_0. \tag{5}$$

Thus, the general thermodynamic pressure can be formulated as

$$\begin{aligned} p &= \sum_{i=1}^{M} n_i \mu_i - f \\ &= p_0 - \sum_{i,j=1}^{M} n_i \nabla \cdot (c_{i,j} \nabla n_j) - \frac{1}{2} \sum_{i,j=1}^{M} c_{ij} \nabla n_i \cdot \nabla n_j, \end{aligned} \tag{6}$$

where $f = f_0 + f_\nabla$.

From equations (4) and (5), we can observe that f_0 connects an EOS and its chemical potential. For multi-component fluids with different EOS, f_0 takes on various forms. For example, in the commonly used Van der Waals EOS, f_0 is expressed as the sum of two terms: an ideal part and an excess part as follows [37].

$$f_0(\mathbf{n}) = f_0^{ideal}(\mathbf{n}) + f_0^{excess}(\mathbf{n}), \tag{7}$$

where

$$f_0^{ideal}(\mathbf{n}) = RT\sum_{i=1}^{M} n_i(\ln n_i - 1), \quad f_0^{excess}(\mathbf{n}) = -nRT\ln(1-bn) - an^2.$$

The Peng-Robinson EOS, which is widely used in the oil reservoir and chemical engineering, is more accurately in the modeling of hydrocarbon mixtures. f_0 takes the following form[11]

$$f_0(\mathbf{n}) = RT\sum_{i=1}^{M} n_i(\ln n_i - 1) - nRT\ln(1-bn) + \frac{an}{2\sqrt{2}b}\ln(\frac{1+(1-\sqrt{2})bn}{1+(1+\sqrt{2})bn}). \tag{8}$$

The definitions of the parameters a and b in the free energy density of van der Waals EOS and P-R EOS are given in Appendix.

Additionally, in the phase field theory, a simplified form of free energy density known as the multiwell potential form is commonly employed in the modeling of multi-component fluid flows[35, 34]. The explicit expression of the multiwell potential free energy density can be represented as follows:

$$f_0(\mathbf{n}) = \sum_{i,j=1}^{M} \beta_{ij}[g(n_i) + g(n_j) - g(n_i + n_j)], \tag{9}$$

where n_i represents the volume fraction of component i in the phase field theory, β_{ij} is a constant, which is related to the surface tension between different component. $g(n_i)$ is typically defined as $g(n_i) = n_i^2(n_i - 1)^2$.

2.2. Governing equation of multi-component mixtures

The mass balance equation for component i is

$$\frac{\partial n_i}{\partial t} + \nabla\cdot(\mathbf{u}n_i) + \nabla\cdot J_i = 0, \tag{10}$$

with

$$J_i = -\sum_{j=1}^{M} M_{ij}\nabla\mu_j, i-1, ..., M,$$

where $\mathbf{u}$ is the average velocity of the mixture, $(M_{ij})_{i,j=1}^{M}$ is the mobility tensor. Based on the Onsager's reciprocal principle and the second law of thermodynamics, it is required that $(M_{ij})_{i,j=1}^{M}$ be symmetric and at least positive semi-definite. Under different conditions, there exist several options for the choice of mobility, which can be found in [34] and [38].

The mass density of the mixture is defined as

$$\rho = \sum_{i=1}^{M} n_i M_{w,i}, \tag{11}$$

where $M_{w,i}$ represents the molar weight of component i. Thus, the mass balance equation of the multi-component two phase fluid system is

$$\frac{\partial \rho}{\partial t} + \nabla \cdot (\rho \mathbf{u}) + \sum_{i=1}^{M} M_{w,i} \nabla \cdot J_i = 0. \tag{12}$$

The momentum balance equation is

$$\begin{aligned} \rho(\frac{\partial \mathbf{u}}{\partial t} + \mathbf{u} \cdot \nabla \mathbf{u}) + \sum_{i=1}^{M} M_{w,i} J_i \cdot \nabla \mathbf{u} = \nabla(\xi - \frac{2}{3}\eta)(\nabla \cdot \mathbf{u} - p) \\ + \nabla \cdot (\eta(\nabla \mathbf{u} + \nabla \mathbf{u}^T)) - \sum_{i,j=1}^{M} \nabla \cdot (c_{ij} \nabla n_i \otimes \nabla n_j) + \mathbf{G}, \end{aligned} \tag{13}$$

where $\mathbf{G}$ is an external body force.

Under the isothermal condition, the gradient of the general pressure and total chemical potential have the following relation,

$$\sum_{i=1}^{M} n_i \nabla \mu_i = \nabla p + \sum_{i,j=1}^{M} \nabla \cdot (c_{ij} \nabla n_i \otimes \nabla n_j).$$

By using the above formula, the momentum conservation equation (13) can be reformulated as a potential form,

$$\rho(\frac{\partial \mathbf{u}}{\partial t} + \mathbf{u} \cdot \nabla \mathbf{u}) + \sum_{i=1}^{M} M_{w,i} J_i \cdot \nabla \mathbf{u} = -\sum_{i=1}^{M} n_i \nabla \mu_i + \nabla \cdot (\eta(\nabla \mathbf{u} + \nabla \mathbf{u}^T) + (\xi - \frac{2}{3}\eta)(\nabla \cdot \mathbf{u})\mathbf{I}) + \mathbf{G}. \tag{14}$$

3. Multiple-distribution-function lattice Boltzmann method for multi-component mixtures

In this study, we develop an efficient lattice Boltzmann method (LBM) that utilizes multiple distribution functions for simulating multi-component mixtures. To begin with, in order to design an efficient LBM, we can reframe the mass balance equations (10) and the momentum conservation equation (14) in the form of a coupled convection-diffusion system as follows.

$$\frac{\partial n_i}{\partial t} + \nabla \cdot (\mathbf{u} n_i) = \nabla \cdot M_{ij} \nabla \mu_j, \quad i = 1, ..., M, \tag{15}$$

$$\frac{\partial \rho u_\alpha}{\partial t} + \nabla \cdot ((\rho u_\alpha + \bar{J}_\alpha)\mathbf{u}) = \nabla \cdot (\eta \nabla u_\alpha) + F_\alpha, \quad \alpha = 1, ..., d, \tag{16}$$

where $\mathbf{u} = (u_\alpha)_{\alpha=1,...,d}$ is the velocity in d-dimensional space. $\bar{\mathbf{J}} = (\bar{J}_\alpha)$ is a flux with $\bar{\mathbf{J}} = -\sum_{i,j=1}^{M} M_{w,i} M_{ij} \nabla \mu_j$ and $\mathbf{F} = \mathbf{F}_s + \mathbf{G} = (F_\alpha)$ with $\mathbf{F}_s = -\sum_{i=1}^{M} n_i \nabla \mu_i$.

3.1. The multiple-distribution-function LBM for mass balance equation

The evolution equation of the LBM with multiple distribution functions for Eq.(15) can be expressed as

$$f_{k,i}(\mathbf{x} + \mathbf{c}_k \delta t, t + \delta t) = f_{k,i}(\mathbf{x}, t) - \Lambda_{ij}[f_{k,j}(\mathbf{x}, t) - f_{k,j}^{eq}(\mathbf{x}, t)] + \delta t S_{k,i}(\mathbf{x}, t), \quad i = 1, ..., M. \tag{17}$$

where $f_{k,i}(\mathbf{x},t)$ is the discrete distribution function for i th component. $\mathbf{c}_k = c\mathbf{e}_k$, $\{\mathbf{e}_k, k = 0, ..., b-1\}$ is the set of discrete velocity directions, $c = \delta x/\delta t$ is the lattice speed, and $[\Lambda_{ij}]_{M\times M}$ is the invertible relaxation matrix.

In (17), $f^{eq}_{k,i}(\mathbf{x},t)$ is the equilibrium distribution function (EDF), which can be written as

$$f^{eq}_{k,i}(\mathbf{x},t) = \omega_k[n_i + \frac{c_k \cdot n_i\mathbf{u}}{c_s^2} + \frac{(\mathbf{c}_k\mathbf{c}_k - c_s^2\mathbf{I}) : (\sum_j c_s^2 K_{ij}\mu_j\mathbf{I} - c_s^2 n_i\mathbf{I})}{2c_s^4}], \tag{18}$$

where $[K_{ij}]_{M\times M}$ is an invertible relaxation matrix. From the Chapman-Enskog (C-E) analysis, we can found that the value of $f^{eq}_{k,i}(\mathbf{x},t)$ is related to the mobility tensor $(M_{ij})^M_{i,j=1}$ and the relaxation matrix $[\Lambda_{ij}]_{M\times M}$. $S_{k,i}(\mathbf{x},t)$ is the auxiliary distribution function, which is defined as

$$S_{k,i}(\mathbf{x},t) = (\delta_{ij} - \frac{\Lambda_{ij}}{2})\frac{\omega_k\mathbf{c}_k \cdot \partial_t(n_j\mathbf{u})}{c_s^2}. \tag{19}$$

In simulations, the DdQq lattice model is used in the present regularized LBM. For example, in the D1Q3 lattice model, $\{\mathbf{c}_0, \mathbf{c}_1, \mathbf{c}_2\} = \{0, c, -c\}$, $\omega_0 = 2/3, \omega_1 = \omega_2 = 1/6$, while for the D2Q9 model, $\{\mathbf{c}_i, i = 0, ..., 8\} = \{(0,0), (\pm c, 0), (0, \pm c), (\pm c, \pm c)\}$, $\omega_0 = 4/9, \omega_{1-4} = 1/9, \omega_{5-8} = 1/36$. Based on the lattice symmetries, the discrete velocities $\mathbf{c}_k$ and weight ω_k satisfy the following isotropic constraints:

$$\begin{cases} \sum\limits_{k=1}^{q} \omega_k = 1, \\ \sum\limits_{k=1}^{q} \omega_k\mathbf{c}_k\mathbf{c}_k = c_s^2\mathbf{I} = c_s^2\delta_{ij}, \\ \sum\limits_{k=1}^{q} \omega_k\mathbf{c}_k = 0, \\ \sum\limits_{k=1}^{q} \omega_k\mathbf{c}_k\mathbf{c}_k\mathbf{c}_k = 0, \\ \sum\limits_{k=1}^{q} \omega_k\mathbf{c}_k\mathbf{c}_k\mathbf{c}_k\mathbf{c}_k\mathbf{c}_k = 0, \\ \sum\limits_{k=1}^{q} \omega_k\mathbf{c}_k\mathbf{c}_k\mathbf{c}_k\mathbf{c}_k\mathbf{c}_k = c_s^4\Delta = c_s^4(\delta_{ij}\delta_{kl} + \delta_{ik}\delta_{jl} + \delta_{il}\delta_{jk}). \end{cases} \tag{20}$$

Applying the above constraints to Eq. (18), the moment conditions can be obtained as

$$\begin{cases} \sum_k f^{eq}_{k,i}(\mathbf{x},t) = n_i(\mathbf{x},t), \\ \sum_k \mathbf{c}_k f^{eq}_{k,i}(\mathbf{x},t) = n_i(\mathbf{x},t)\mathbf{u}, \\ \sum_k \mathbf{c}_k\mathbf{c}_k f^{eq}_{k,i}(\mathbf{x},t) = \sum_j c_s^2 K_{ij}\mu_j\mathbf{I}, \\ \sum_k S_{k,i}(\mathbf{x},t) = 0, \\ \sum_k \mathbf{c}_k S_{k,i}(\mathbf{x},t) = (\delta_{ij} - \frac{\Lambda_{ij}}{2})\partial_t(n_j\mathbf{u}). \end{cases} \tag{21}$$

The molar density or volume fraction n_i is then calculated by

$$n_i(\mathbf{x},t) = \sum_k f_{k,i}(\mathbf{x},t). \tag{22}$$

3.2. The multiple-distribution-function LBM for the potential form momentum conservation equation

The evolution equations of the LBM with multiple distribution functions for Eq. (16) can be expressed as

$$\begin{aligned} h_{k,\alpha}(\mathbf{x}+\mathbf{c}_k\delta t, t+\delta t) =& h_{k,\alpha}(\mathbf{x},t) - \bar{\Lambda}_{k,j}[h_{j,\alpha}(\mathbf{x},t) - h^{eq}_{j,\alpha}(\mathbf{x},t)] \\ &+ \delta t[G_{k,\alpha}(\mathbf{x},t) + F_{k,\alpha}(\mathbf{x},t) + \frac{\delta t}{2}\bar{D}_k F_{k,\alpha}(\mathbf{x},t)], \quad \alpha = 1, ..., d, \end{aligned} \tag{23}$$

where $h_{k,\alpha}(\mathbf{x},t)$ is the discrete distribution function for α-th velocity, $\bar{D}_k = \partial_t + \gamma \mathbf{c}_k \cdot \nabla$, with the parameter $\gamma \in \{0, 1\}$, and $[\bar{\Lambda}_{k,j}]_{b\times b}$ is the invertible collision matrix. It has been pointed out in [36] that to recover the correct macroscopic equations, the collision matrix should satisfy the following conditions,

$$\sum_i \mathbf{e}_i \bar{\Lambda}_{ik} = s_0 \mathbf{e}_k, \sum_i \mathbf{c}_i \bar{\Lambda}_{ik} = s_1 \mathbf{c}_k, \tag{24}$$

where $\mathbf{e} = (1, 1, ..., 1)$ and s_0, s_1 are eigenvalues of the collision matrix $\bar{\Lambda}$. In (23), $h^{eq}_{k,\alpha}(\mathbf{x},t)$ is the equilibrium distribution function, $G_{k,\alpha}(\mathbf{x},t)$ and $F_{k,\alpha}(\mathbf{x},t)$ are the auxiliary distribution function and the distribution function for source term F_α, respectively. They are defined by

$$\begin{aligned} h^{eq}_{k,\alpha}(\mathbf{x},t) &= \omega_k[\rho u_\alpha + \frac{\mathbf{c}_k \cdot (\rho u_\alpha + \bar{J}_\alpha)\mathbf{u}}{c_s^2}], \\ G_{k,\alpha}(\mathbf{x},t) &= (1 - \frac{s_1}{2})\omega_k \mathbf{c}_k \cdot \frac{\partial_t[(\rho u_\alpha + \bar{J}_\alpha)\mathbf{u}] + c_s^2 u_\alpha \nabla \rho}{c_s^2}, \\ F_{k,\alpha}(\mathbf{x},t) &= \omega_k F_\alpha. \end{aligned} \tag{25}$$

By using the isotropic constraints (20), the following moments can be obtained.

$$\begin{cases} \sum_k h^{eq}_{k,\alpha}(\mathbf{x},t) = \rho u_\alpha, \\ \sum_k \mathbf{c}_k h^{eq}_{k,\alpha}(\mathbf{x},t) = (\rho u_\alpha + \bar{J}_\alpha)\mathbf{u}, \\ \sum_k \mathbf{c}_k \mathbf{c}_k h^{eq}_{k,i}(\mathbf{x},t) = c_s^2 \rho u_\alpha \mathbf{I}, \\ \sum_k G_{k,\alpha}(\mathbf{x},t) = 0, \\ \sum_k \mathbf{c}_k G_{k,\alpha}(\mathbf{x},t) = (1 - \frac{s_1}{2})\{\partial_t[(\rho u_\alpha + \bar{J}_\alpha)\mathbf{u}] + c_s^2 u_\alpha \nabla \rho\}, \\ \sum_k F_{k,\alpha} = F_\alpha, \\ \sum_k \mathbf{c}_k F_{k,\alpha} = 0. \end{cases} \tag{26}$$

The macroscopic velocity u_α is then calculated by

$$u_\alpha = \sum_k h_{k,\alpha}(\mathbf{x},t)/\rho. \tag{27}$$

4. Numerical experiments

In this section, we will conduct a series of numerical experiments to showcase the effectiveness of the proposed MDF-LBM.

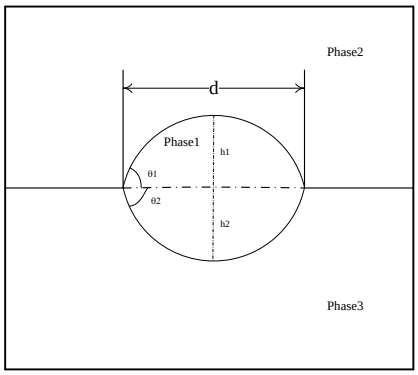

Figure 1: The schematic of the spreading of a liquid lens.

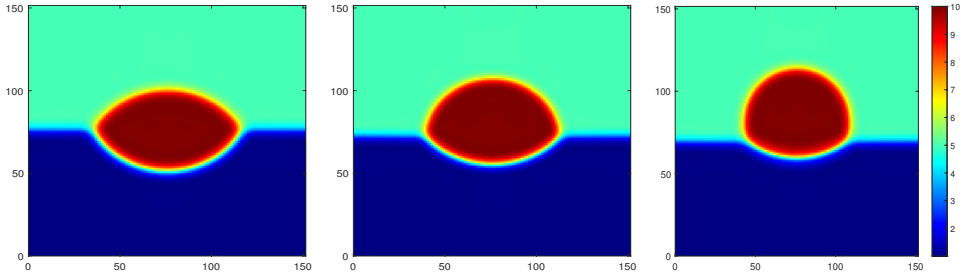

(a) (b) (c)

Figure 2: The equilibrium shapes of liquid by ternary fluids, $\rho_1 : \rho_2 : \rho_3 = 10 : 5 : 1$. (a) $\sigma_{12} : \sigma_{13} : \sigma_{23} = 1 : 1 : 1$, (b) $\sigma_{12} : \sigma_{13} : \sigma_{23} = 1 : \sqrt{2} : 1$, (c) $\sigma_{12} : \sigma_{13} : \sigma_{23} = 1 : \sqrt{3} : 1$.

4.1. Spreading of a liquid lens

To evaluate the accuracy of the proposed MDF-LBM, we simulate a three-phase benchmark problem that involves the spreading of a liquid lens between two immiscible fluids. This particular benchmark problem has attracted the attention of numerous researchers due to the availability of theoretical solutions [39, 40, 41, 34]. The schematic of the problem is depicted in Fig. 1. Once the system reaches equilibrium, the droplet representing phase 1 takes the shape of a floating liquid lens on the interface of phase 3. The equilibrium contact angles θ_1 and θ_2 can then be quantitatively estimated using Neumann's law [42]:

$$\cos(\theta_1) = \frac{\sigma_{12}^2 + \sigma_{23}^2 - \sigma_{13}^2}{2\sigma_{12}\sigma_{23}}, \quad \cos(\theta_2) = \frac{\sigma_{13}^2 + \sigma_{23}^2 - \sigma_{12}^2}{2\sigma_{13}\sigma_{23}},$$

where σ_{ij} represents the surface tension between phase i and phase j. The distance between two triple junctions d and the heights (h_i) can be determined by

$$d = 2\sqrt{A \Big/ \sum_i \frac{1}{\sin(\theta_i)}\left(\frac{\theta_i}{\sin\theta_i} - \cos\theta_i\right)}, \quad h_i = \left(\frac{d}{2}\right)\frac{1-\cos\theta_i}{\sin\theta_i}, \quad i = 1, 2,$$

where A is the lens area.

Table 1: The length d, h_1 and h_2 at equilibrium state with different surface tension ratios.

$\sigma_{12}:\sigma_{13}:\sigma_{23}$	Analytical solutions			Numerical solutions			Relative errors		
	d	h_1	h_2	d	h_1	h_2	d	h_1	h_2
$1:1:1$	83.10	23.99	23.99	82.63	24.43	23.59	0.89%	1.83%	1.67%
$1:\sqrt{2}:1$	72.67	36.34	15.05	73.14	36.08	15.26	0.65%	0.72%	1.39%
$1:\sqrt{3}:1$	55.05	47.67	7.38	53.67	46.82	7.22	2.51%	1.78%	2.17%

In the simulation, the initial conditions are set as

$$\begin{aligned} n_1(x,y) &= 0.5 + 0.5\tanh\frac{2[R-\sqrt{(x-x_c)^2+(y-y_c)^2}]}{D}, \\ n_2(x,y) &= \max[0.5 + 0.5\tanh\frac{2(y-y_c)^2}{D} - n_1(x,y), 0], \\ n_3(x,y) &= 1.0 - n_1(x,y) - n_2(x,y), \end{aligned}$$

where $R = 30$ is the radius of the circular lens, $D = 5$ is the thickness of the characterisitic interface and (x_c, y_c) is the center of the circular droplet. The computational domain is discretized using a mesh grid of 150×150. Periodic boundary conditions are applied in the x-direction, while non-slip boundary conditions are enforced at the top and bottom boundaries. In order to maintain consistency, the dimensionless fluid density ratios are set as $\rho_1 = 10$, $\rho_2 = 5$ and $\rho_3 = 1$. Additionally, the surface tension is specified as $\sigma_{12} = 0.01$, and three distinct cases of surface tension ratios of $\sigma_{12}:\sigma_{13}:\sigma_{23} = 1:1:1$, $\sigma_{12}:\sigma_{13}:\sigma_{23} = 1:\sqrt{2}:1$ and $\sigma_{12}:\sigma_{13}:\sigma_{23} = 1:\sqrt{3}:1$ are investigated.

Fig. 2 displays the equilibrium states of the liquid lens at various surface tension ratios. The results highlight that the equilibrium shape of the liquid lens assumes distinct patterns depending on the surface tension ratio, with an increasing tendency towards spherical morphology as σ_{13} rises. To quantitatively evaluate the accuracy of the proposed MDF-LBM, the equilibrium length (d) and height of the liquid lens (h_1, h_2) are measured and compared with theoretical solutions, as presented in Table 1. Notably, the numerical results for both length d and height (h_1, h_2) align well with the anticipated theoretical values, exhibiting relative differences of d, h_1 and h_2 less than 2.51%. This agreement substantiates the validity of the proposed MDF-LBM.

4.2. Bubble rise in stratified layers

The phenomenon of bubble rising or falling in systems with distinct phases is extensively observed in various environmental and industrial applications, such as microfluidics, ink-jet printing, and gas-liquid reactors. Consequently, numerous researchers have been drawn towards exploring this area [41, 44, 45, 46, 47]. To ascertain the capability of the proposed MDF-LBM, a numerical investigation into the dynamics of a gas bubble in a two-layer liquid is conducted. The configuration of this particular problem is illustrated in Fig. 3. In this setup, a circular bubble with a radius of $R = 20$ is introduced into the lower liquid layer, which is denser and occupied by fluid 3. The upper liquid layer, on the other hand, is filled with fluid 2. A meshgrid

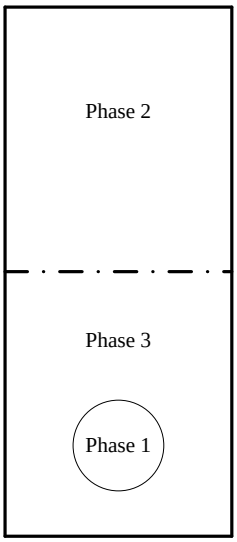

Figure 3: Configuration of the bubble rise in stratified layers.

of $Nx \times Ny = 160 \times 480$ is employed for the simulation, while periodic and non-slip boundary conditions are implemented in the horizontal and vertical directions respectively. In addition, the initial data is set to

$$n_1(x,y) = 0.5 + 0.5\tanh\frac{2[R - \sqrt{(x-x_c)^2 + (y-y_c)^2}]}{D}, \tag{28a}$$

$$n_2(x,y) = [0.5 + 0.5\tanh\frac{2(y-y_0)}{D}] \times (1 - n_1), \tag{28b}$$

$$n_3(x,y) = 1.0 - n_1 - n_2, \tag{28c}$$

where $(x_c, y_c) = (Nx/2, Ny/8)$ is the center of the bubble and $y_0 = \frac{1}{2}Ny$ is the position of the horizontal interface between fluid 2 and 3. The other physical parameters are chosen as $\rho_1 = 1.0$, $\rho_2 = 3.0$, $\rho_3 = 6.0$, the surface tensions are $\sigma_{12} = \sigma_{13} = 0.01$, $D = 3.0$, the gravitational force $g = 2.0 \times 10^{-5}$. The non-dimensional parameter Bond number ($Bo = g\Delta\rho(2R)^2/\sigma_{23}$) is introduced, where $\Delta\rho = \rho_3 - \rho_1$ is density difference. The influence of different values of $Bo = 5, 10, 20$ on the dynamic behavior of bubble rising is examined in this work.

Fig. 4 displays the temporal evolution of the phase interfaces at various moments for different values of Bo. The lattice scale time t is appropriately rescaled by $\sqrt{2R/g}$. It is observed that the gas bubble initiates an upward motion due to buoyancy, acquiring a crescent shape as time progresses. The interface between fluid 2 and 3 exhibits notable susceptibility to deformation at $Bo = 20$. In other words, when Bo attains a larger value, the ease with which the bubble passes through the fluid 2 and 3 interface becomes more pronounced. This behavior stems from the decreased significance of Bo, consequently augmenting the role of surface tension, which in turn impedes the ascent of the gas bubble through the fluid 2 and 3 interface. These numerical findings are qualitatively consistent with the results reported in previous studies [34, 35]. Moreover, to demonstrate the ability of the proposed MDF-LBM to ensure the conservation of mass for each phase, the temporal history of the mass for each phase is presented in Fig. 5. It can be distinctly

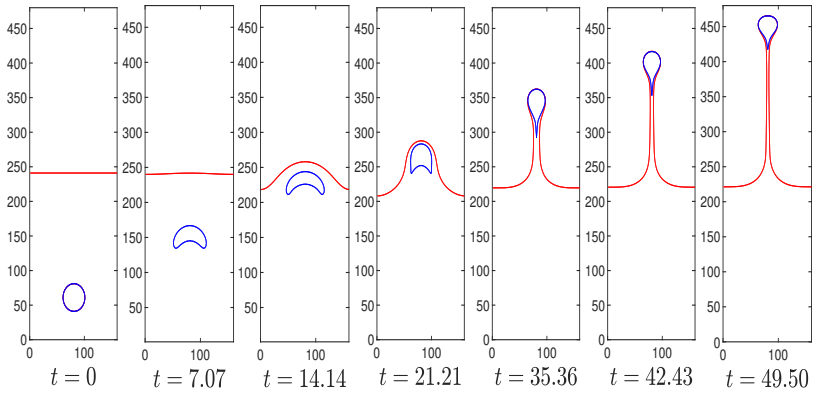

(a)

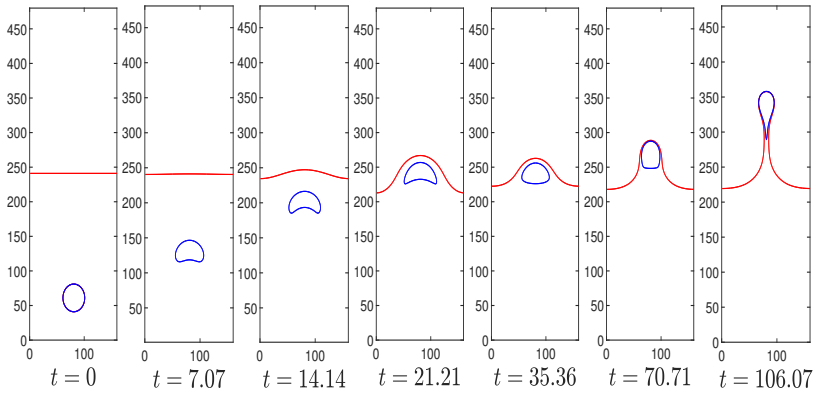

(b)

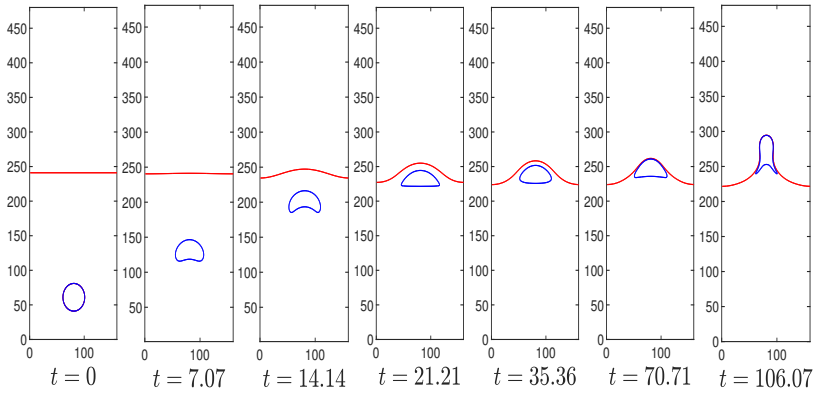

(c)

Figure 4: Time evolution of bubble rising in stratified layers at different moments. (a) $Bo = 20$; (b) $Bo = 10$; (c) $Bo = 5$.

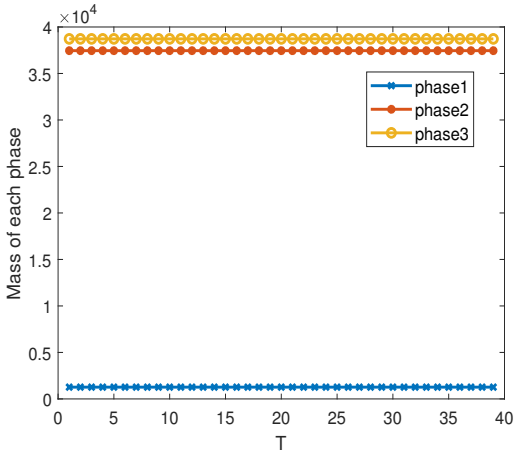

Figure 5: Mass evolution with time of each phase.

observed that the mass of each phase remains constant as time progresses, indicating the fulfillment of the mass conservation law.

4.3. Calculation of the surface tension of two-component hydrocarbon mixture

A thorough comprehension of the phase behavior exhibited by multi-component and multi-phase hydrocarbon fluids holds significant importance in the petroleum industry. In order to assess the efficacy of the proposed MDF-LBM in accurately representing real states of hydrocarbon mixtures, a simulation is conducted on a binary component two-phase fluid system composed of methane (CH_4) and n-decane ($nC_{10}H_{22}$). Throughout the numerical simulation process, the present MDF-LBM incorporates the widely employed P-R free energy model, which finds extensive application in reservoir engineering domains such as subsurface CO_2 sequestration and shale gas reservoirs. The thermodynamic properties of CH_4 and $nC_{10}H_{22}$ components, pertinent to hydrocarbon systems, are presented in Table 2.

The numerical simulation is conducted within a three-dimensional cube, with each side measuring a length of $L = 10^{-8}$ meters. The D3Q15 lattice model is employed, and a periodic boundary condition is applied to the entire boundary. The computational domain is discretized using a uniform cubic mesh of $140 \times 140 \times 140$. Initially, the liquid phase of the substances, maintained at a saturated pressure of 450 K, is confined within a subregion of the cube denoted by $(\frac{3}{16}L, \frac{7}{16}L), (\frac{9}{16}L, \frac{13}{16}L)$. The remaining portion of the domain is filled with the gas phase of the binary mixture, subject to the same conditions. The initial values for methane and n-decane at various temperatures can be retrieved from the specified reference [48]. The iso-surface of the molar density of the mixture at different instances is visualized in Fig. 6. Analysis of the figure reveals that the initially distinct droplets assume a spherical shape and commence merging as a result of surface tension. With the passage of time, the individual droplets coalesce, ultimately transforming into a singular, perfectly spherical entity.

To make a quantitative study of the two phase binary component fluid mixture, the surface tension is

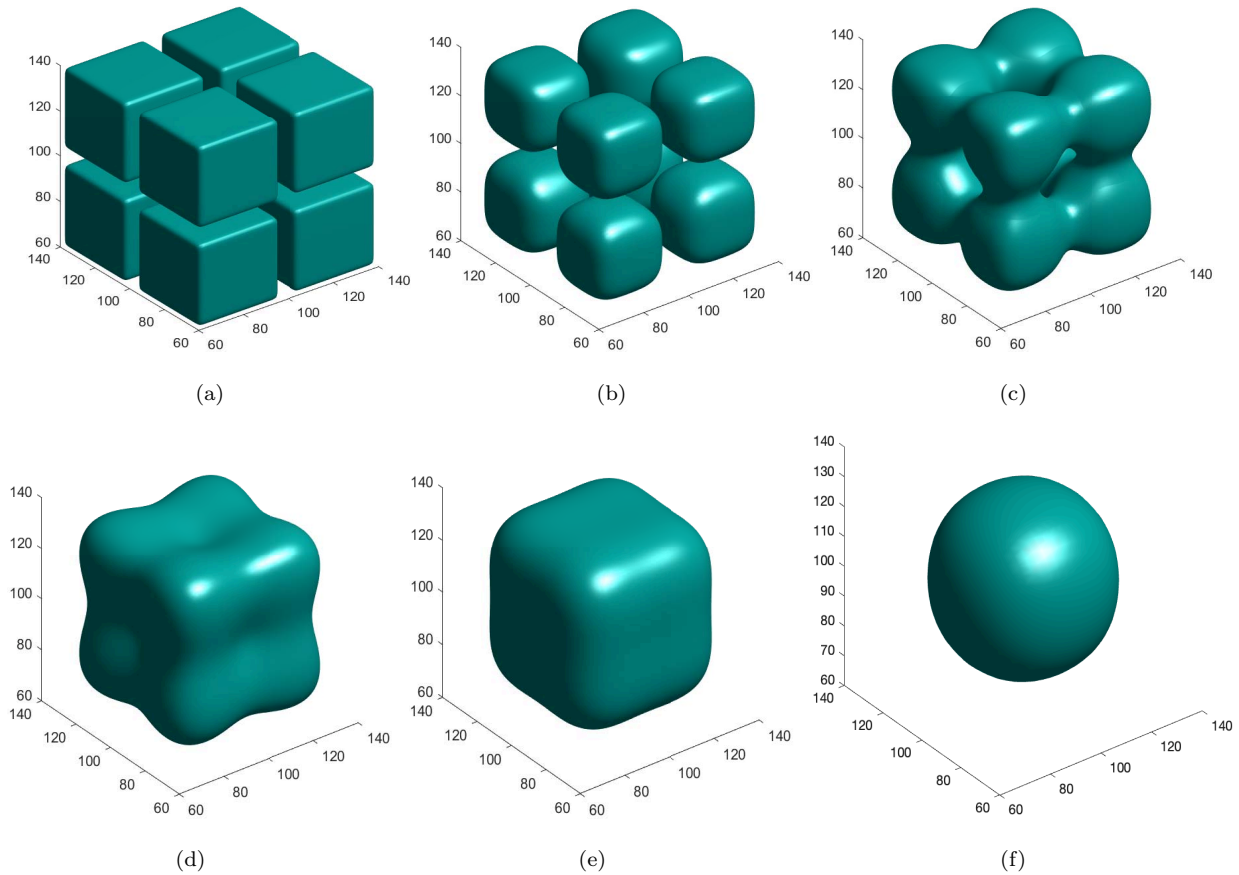

Figure 6: Time evolution of the multi-droplet. (a) t=0, (b) t=100, (c) t=500, (d) t=800, (e) t=1200, (f) t=5000.

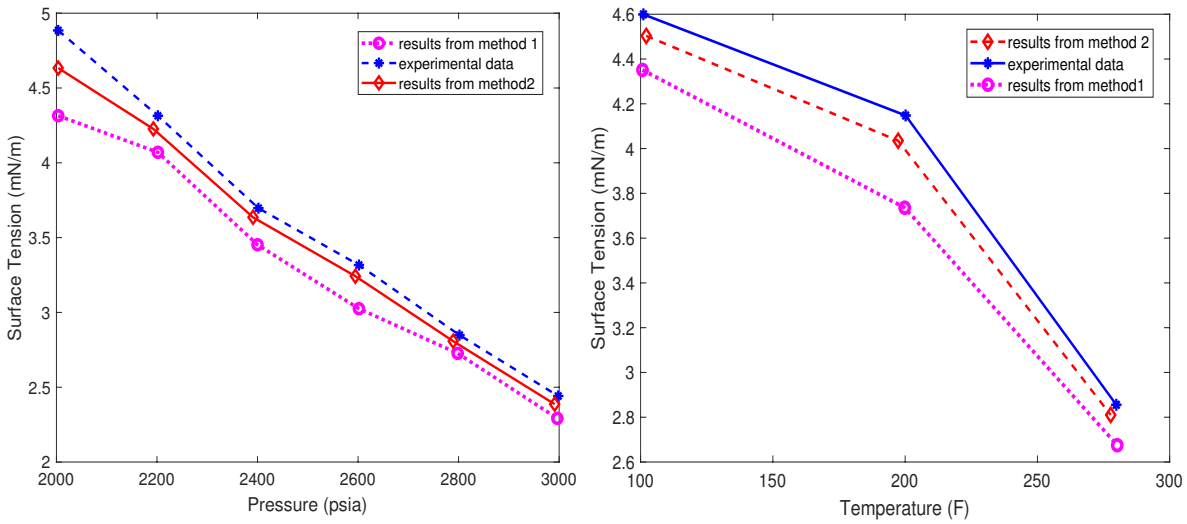

Figure 7: Comparison of surface tension between numerical results and experimental data: at temperature $T = 280^oF$ (left); at pressure $P_0 = 2800psia$ (right).

Table 2: The thermodynamic properties of hydrocarbon components.

Component	Critical temperature T_c, K	Critical pressure P_c, MPa	Boiling point T_b, K	Accentric factor ω_i
CH_4	190.74	4.595	111.63	0.0104
$nC_{10}H_{22}$	617.7	2.099	447.3	0.489

numerically predicted by the present LBM. The surface tension is computed through the formula

$$\sigma_{sur} = \frac{F(\mathbf{n}) - F(\mathbf{n}_{initial})}{A},$$

where A is the cross surface area of the liquid drop. When we calculate the area A, the thickness of the interface needs to be taken into account. The calculate area A is determined as the weighted mean of the area of different substances, $A = \sum_i \omega_i A_i$, where $\omega_i = N_i / \sum_i N_i$ and A_i represents the area of the $i-$th component. As pointed out in the reference [48], there are two different approaches to calculate the area A_i. The first method, which is termed as method 1, is to use the interface width L to get the radius of the droplet at the equilibrium state as $r = \frac{1}{2}L + r_0$ (Assuming that the area of the square droplet at the initial state is A_s, $r_0 = \sqrt{\frac{2A_s}{\pi}}$). The second method (method 2) is set the distance from the middle point of the interface to the middle point of the pure liquid droplet as the radius to get the area A_i.

We compute the interface tension with temperature 280^oF and pressure from 2000 to 3000 psia every 200 psia. And it is also computed at constant pressure 2800 psia and temperatures at 100^oF, 200^oF and 280^oF, respectively. Fig. 7 shows interface tensions calculated by these two approaches and compare with the laboratory data [37, 49]. We can see that interface tensions obtained by the method 2 are much better than those method 1 due to the involving interface width.

5. Conclusion

This paper presents a numerical study of immiscible and partially miscible multi-phase and multi-component fluid systems using the proposed MDF-LBM method. We modified the second order moments condition to handle the cross diffusion term in the CH type mass conservation equation. Additionally, we reformulated the momentum transport equation as a potential form based on the relationship between total chemical potential and thermodynamic pressure. The hydrodynamic equations were obtained by coupling the mass conservation equations of each component with the potential form momentum transport equation. To avoid redundant density calculations, the MDF-LBM method was developed for the momentum transport equation. Several numerical experiments were conducted to evaluate the capabilities of the proposed MDF-LBM method, including the spreading of a liquid lens, bubble rise in stratified layers, and 3D multi-component two-phase hydrocarbon mixtures. The numerical results of the spreading of a liquid lens showed good agreement with analytical solutions and reported data. Additionally, the mass conservation property of the proposed MDF-LBM method was examined in the numerical simulation of bubble rise in stratified layers, effectively capturing the phase behavior. Finally, realistic hydrocarbon mixtures of methane and n-decane

were simulated using the multi-component P-R free energy model. A more accurate method for calculating the surface tension of the multi-component system was presented, and the 3D numerical results exhibited improved agreement with laboratory experimental data.

Acknowledgments

This work is supported by the CAS AMSS-PolyU Joint Laboratory of Applied Mathematics. Z. Qiao's work is partially supported by the Hong Kong Research Grants Council (RFS Project No. RFS2021-5S03 and GRF project No. 15302122) and the Hong Kong Polytechnic University internal grant No. 1-9B7B. X. Yang's work is partially supported by the Natural Science Foundation of China (Grant No. 12372286). Y. Zhang's work is partially supported by the Natural Science Foundation of China (Grant No. 12301554) and the Natural Science Foundation of Jiangsu Province (Grant No. BK20220368), Natural Science Fund for Colleges and Universities in Jiangsu Province (Grant No. 22KJD110003)

Appendix A. Parameters of the P-R EOS

For multi-component fluid systems, $a = a(T)$ is the pressure correction coefficient and $b = b(T)$ is the volume correction coefficient, which are given by

$$a\,(T) = \sum_{i=1}^{M}\sum_{j=1}^{M} y_i y_j (a_i a_j)^{\frac{1}{2}}(1-k_{ij}), \qquad b(T) = \sum_{i=1}^{M} y_i b_i.$$

Here, $y_i = n_i/n$ is the mole fraction of component i, k_{ij} is the binary interaction coefficient for the energy parameters. a_i and b_i are defined as follows,

$$a_i(T) = 0.45724\frac{R^2}{T_{ci}^2}(1+m_i(1-\sqrt{\frac{T}{T_{ci}}}))^2, \quad b_i = 0.7780\frac{RT_{ci}}{P_{ci}},$$

where, T_{ci} and P_{ci} are properties of the i-th substance which represent the critical temperature and critical pressure, respectively. m_i is a function of the acentric factor ω_i of the substance

$$m_i = 0.37464 + 1.54226\omega_i - 0.26992\omega_i^2, \quad \omega_i \le 0.49,$$

$$m_i = 0.379642 + 1.485030\omega_i - 0.164423\omega_i^2 + 0.016666\omega_i^3, \quad \omega_i > 0.49.$$

The acentric parameter ω_i can be computed by using critical temperature T_{ci}, critical pressure P_{ci} and the normal boiling point T_{bi}:

$$\omega_i = \frac{3}{7}(\frac{\log_{10}(\frac{P_{ci}}{14.695\mathrm{PSI}})}{\frac{T_{ci}}{T_{bi}}-1}) - 1.$$

References

[1] S. Sun and M. F.Wheeler. Symmetric and nonsymmetric discontinuous galerkin methods for reactive transport in porous media. SIAM J. Numer. Anal., 43 (2005), 195-219.

[2] J. Moortgat, S. Sun, and A. Firoozabadi. Compositional modeling of three-phase flow with gravity using higher-order finite element methods, Water Resour. Res., 47 (2011), W05511.

[3] X. Chen, G. Hu. Multiphase flow in mircrofluidic devices. Adv. Appl. Mech., 45 (2015), 201503.

[4] S. Mukherjee, H. Gomez. Flow and mixing dynamics of phase-transforming multicomponent fluids. Appl. Phys. Lett., 115 (2019), 104101.

[5] M. Sussman, P. Smereka, S. Osher. A level set approach for computing solutions to incompressible two-phase flow, J. Comput. Phys. 114 (1994), 146-159.

[6] G. Tryggvason, B. Bunner, A. Esmaeeli. A front tracking method for computations of multiphase flow, J. Comput. Phys., 169 (2001), 708-759.

[7] C.W. Hirt, B.D. Nichols. Volume of fluid (VOF) method for the dynamics of free boundaries, J. Comput. Phys., 39 (1989), 201-225.

[8] D.M. Anderson, G.B. Mcfadden, A.A. Wheeler. Diffuse-interface methods in fluid mechanics, Annu. Rev. Fluid Mech., 30 (1998), 139-165.

[9] F. Boyer, C. Lapuerta, S. Minjeaud, B. Piar, and M. Quintard. Cahn-Hilliard/Navier-Stokes model for the simulation of three-phase flows. Transp. Porous Media, 82 (2010), 463-483.

[10] V. E. Badalassi, H. D. Ceniceros, and S. Banerjee. Computation of multiphase systems with phase field models. J. Comput. Phys., 190 (2003), 371-397.

[11] Z. Qiao and S. Sun. Two-phase fluid simulation using a diffuse interface model with Peng-Robinson equation of state. SIAM J. Sci. Comput., 36 (2014), B708-B728.

[12] S. Chen, G. Doolen, Lattice Boltzmann method for fluid flows, Annu. Rev. Fluid Mech., 30 (1998), 329-364.

[13] C. Aidun, J. Clausen. Lattice Boltzmann method for complex flows, Annu. Rev. Fluid Mech., 42 (2010), 372-439.

[14] Z. Guo, C. Shu. Lattice Boltzmann method and its applications in engineering. Singapore: World Scientific Publishing Co. Pte. Ltd., 2013.

[15] P. Lallemand, L. Luo, Theory of the lattice Boltzmann method: Dispersion, dissipation, isotropy, Galilean invariance, and stability, Phys. Rev. E, 61 (2000), 6546.

[16] X. He, S. Chen, R. Zhang, A lattice Boltzmann scheme for incompressible multiphase flow and its application in simulations of Rayleigh-Taylor instability, J. Comput. Phys., 152 (1999), 652-663.

[17] H. B. Huang, M. Sukop, X. Y. Lu. Multiphase lattice Boltzmann methods: Theory and application. Oxford: JohnWiley & Sons, Ltd., 2015.

[18] L. Chen, Q. Kang, Y. Mu, Y. L. He, W. Q. Tao. A critical review of the pseudopotential multiphase lattice Boltzmann model: Methods and applications. International Journal of Heat and Mass Transfer, 76 (2014), 210-236.

[19] Q. Li, K. H. Luo, Q. J. Kang, Y. L. He, Q. Chen, Q. Liu. Lattice Boltzmann methods for multiphase flow and phase-change heat transfer. Progress in Energy and Combustion Science, 52 (2016), 62-105.

[20] A. Fakhari, D. Bolster, L. S. Luo. A weighted multiple-relaxation-time lattice Boltzmann for multiphase flows and its application to partial coalescence cascades. J. Comput. Phys., 341 (2017), 22-43.

[21] Z. H. Qiao, X. G. Yang, Y. Z. Zhang. Mass conservative lattice Boltzmann scheme for a three-dimensional diffuse interface model with Peng-Robinson equation of state. Phys. Rev. E, 98 (2018), 023306.

[22] Z. H. Qiao, X. G. Yang, Y. Z. Zhang. Thermodynamic-consistent multiple-relaxation-time lattice Boltzmann equation model for two-phase hydrocarbon fluids with Peng-Robinson equation of state. Int. J. Heat Mass Trans., 141 (2019), 1216-1226.

[23] X. Shan, H. Chen, Lattice boltzmann model for simulating flows with multiple phases and components, Phys. Rev. E, 47 (1993), 1815-1819.

[24] X. Shan, H. Chen, Simulation of nonideal gases and liquid gas phase-transition by the lattice Boltzmann equation, Phys. Rev. E, 49 (1994), 2941-2948.

[25] M. Swift, E. Orlandini, W. Osborn, J. Yeomans, Lattice Boltzmann simulations of liquid gas and binary fluid systems, Phys. Rev. E, 54 (1996), 5041-5052.

[26] M. R. Swift, W. R. Osborn, J. M. Yeomans, Lattice Boltzmann simulation of nonideal fluids, Phys. Rev. Lett. 75 (1995) 830-833.

[27] X. He, S. Chen, and R. Zhang. A lattice Boltzmann scheme for incompressible multiphase flow and its application in simulation of RayleighCTaylor instability. J. Comput. Phys., 152 (1999), 642-663.

[28] T. Lee and C.-L. Lin. A stable discretization of the lattice Boltzmann equation for simulation of incompressible two-phase flows at high density ratio. J. Comput. Phys., 206 (2005), 16-47.

[29] H. Deng, K. Jiao, Y. Hou, J. Park, Q. Du. A lattice Boltzmann model for multi-component two-phase gas-liquid flow with realistic fluid properties. Intational Journal of Heat and Mass Transfer, 128 (2019), 536-549.

[30] C. Peng, L. F. Ayala, O. M. Ayala. A thermodynamically consistent pseudo-potential lattice Boltzmann model for multi-component, multiphase, partially miscible mixtures. J. Comput. Phys., 429 (2021), 110018.

[31] M. Wöhrwag, C. Semprebon, Moqaddam A. Mazloomi, I. Karlin, H. Kusumaatmaja. Ternary Free-Energy Entropic Lattice Boltzmann Model with a High Density Ratio. Physcal Review Letter, 120 (2018), 234501.

[32] K. S. Ridl, A. J. Wagner. Lattice Boltzmann simulation of mixtures with multicomponent van der Waals equation of state. Physical Review E, 98 (2018), 043305.

[33] M. Soomro, L. F. Ayala, C. Peng, O. M. Ayala. Fugacity-based lattice Boltzmann method for multi-component multiphase systems. Physical Review E, 107 (2023), 015304.

[34] X. L. Yuan, B. C. Shi, C. Z. Zhan. A phase-field-based lattice Boltzmann model for multiphase flows involving N immiscible incompressible fluids. Phys. Fluids, 34 (2022), 023311.

[35] L. Zheng, S. Zheng and Q. Zhai. Reduction-consistent Cahn-Hilliard theory based lattice Boltzmann equation method for N immiscible incompressible fluids. Physica A, 574 (2021), 126015.

[36] Z. H. Chai, B. C. Shi, C. J. Zhan. Multiple-distribution-function lattice Boltzmann method for convection-diffusion-system-based incompressible Navier-Stokes equations. Phys. Rev. E, 106 (2022), 055305.

[37] X. L. Fan, J. K. Kou, Z. H. Qiao, S. Y. Sun. A componentwise convex splitting scheme for diffuse interface models with van der Waals and Peng-Robinson equation of state. SIAM J. Sci. Comput., 39 (2017), B1-B28.

[38] J. S. Kou, S. Y. Sun. Thermodynamically consistent modeling and simulation of multi-component two-phase flow with partial miscibility. Comput. Methods Appl. Mech. Engrg., 331 (2018), 623-649.

[39] F. Boyer and C. Lapuerta. Study of a three component Cahn-Hilliard flow model. ESAIM: Math. Modell. Numer. Anal. 40 (2006), 653-687.

[40] T. J. Spencer, I. Halliday, and C. M. Care. Lattice Boltzmann equation method for multiple immiscible continuum fluids. Phys. Rev. E, 82 (2010), 066701.

[41] S. Dong. An efficient algorithm for incompressible N-phase flows. J. Comput. Phys., 276 (2014), 691-728.

[42] J. S. Rawlinson, B. Widom, The Molecular Theory of Capillarity, Clarendon Press, Oxford, 1982.

[43] Y. Zu and S. He, Phase-field-based lattice Boltzmann model for incompressible binary fluid systems with density and viscosity contrasts. Phys. Rev. E, 87 (2013), 043301.

[44] L. Amaya-Bower, T. Lee. Single bubble rising dynamics for moderate Reynolds number using lattice Boltzmann method, Comput. Fluids 39 (2010), 1191-1207.

[45] J. Qian and C. K. Law. Regimes of coalescence and separation in droplet collision. J. Fluid Mech., 331 (1997), 59-80.

[46] S. Anwar. Lattice Boltzmann modeling of buoyant rise of single and multiple bubbles, Comput. Fluids 88 (2013), 430-439.

[47] H. Hinterbichler, C. Planchette, and G. Brenn. Ternary drop collisions. Experiments in Fluids, 56 (2015), 190.

[48] Z. H. Qiao, S. Y. Sun, T. Zhang, Y. Z. Zhang. A New Multi-Component Diffuse Interface Model with Peng-Robinson Equation of State and Its Scalar Auxiliary Variable Approach. Commun. Comput. Phys., 26 (2019), 1597-1616.

[49] R. Amin and T. N. Smith. Interfacial tension and spreading coeffcient under reservoir conditions. Fluid Phase Equilibr., 142 (1998) 231-241.